Chemical structures of the $Cu(In,Ga)Se_2$/Mo and $Cu(In,Ga)(S,Se)_2$/Mo interfaces

M. Bär,* L. Weinhardt, and C. Heske
Department of Chemistry, University of Nevada, Las Vegas (UNLV), 4505 S. Maryland Parkway, Las Vegas, Nevada 89154-4003, USA

S. Nishiwaki and W. N. Shafarman
Institute of Energy Conversion (IEC), University of Delaware, Newark, 451 Wyoming Road, Newark, Delaware 19716, USA
(Received 11 April 2008; published 5 August 2008)

Using a suitable lift-off technique, we have investigated the chemical properties of the interface between Mo and chalcopyrite compound semiconductors by x-ray photoelectron spectroscopy and x-ray excited Auger-electron spectroscopy. By a systematic comparison of interfaces between S-free [$Cu(In,Ga)Se_2$ (CIGSe)] as well as S-containing [$Cu(In,Ga)(S,Se)_2$ (CIGSSe)] chalcopyrites and Mo, we find that the chemical structure at the CIG(S)Se/Mo interface is strongly influenced by the presence or absence of S. We observe an interfacial $MoSe_2$ [$Mo(S_ZSe_{1-Z})_2$] layer formed between CIGSe [CIGSSe] and the Mo layer. The $Mo(S_ZSe_{1-Z})_2$ layer appears significantly thinner than the $MoSe_2$ layer and exhibits a different S/(S+Se) ratio [$Z=0.9(1)$] than the CIGSSe back side [0.5(7)], giving insight into the "competition" between S and Se during contact formation. Furthermore, we find a significant Ga accumulation at the Mo back contact, which points to pronounced chemical interactions during the formation of the CIG(S)Se/Mo interface.

DOI: 10.1103/PhysRevB.78.075404 PACS number(s): 68.35.Fx

I. INTRODUCTION

Chalcopyrite compound semiconductors [$Cu(In_{1-X}Ga_X)(S_YSe_{1-Y})_2$ ("CIGSSe")] have gained significant attention as promising absorber materials in thin-film solar cells.[1] CIGSSe-based devices are based on a relatively simple transparent conductive oxide (TCO)/buffer/CIGSSe/back-contact/substrate structure. Many different TCOs and buffer materials are being used; in contrast, Mo is the almost exclusively used back-contact material. Initially, Au was successfully used as a contact,[2] but later Mo was chosen because of lower costs with no loss in efficiency. The main demand for the back contact is to provide a low series resistance and an Ohmic contact to the absorber layer (which is believed to be optimal). For the interface between S-free ($Y=0$) $Cu(In,Ga)Se_2$ ("CIGSe") and Mo some authors[3–5] find an Ohmic contact, whereas others[6,7] find a Schottky barrier. One of the main reasons for this discrepancy is that it is difficult to investigate the real CIG(S)Se/Mo interface, since the formation of this interface takes place during the CIG(S)Se deposition and cannot be viewed as final until the preparation is completed. In particular, the CIG(S)Se film is held at elevated temperatures (550 °C) in Se and/or S-containing atmospheres, which is believed to also alter the properties of the Mo layer. It has been found or suggested that a layer of $MoSe_2$ (MoS_2) exists between CIGSe ($CuInS_2$) and Mo.[4,8–16] It is even suspected that this layer is responsible for the Ohmic contact at the CIGSe/Mo interface.[4]

The properties of the CIG(S)Se/Mo interface result from a complex interplay of different factors. These are the directly accessible deposition parameters of the Mo, which have been found to influence the conductivity and the adhesion on the substrate,[17] as well as the less accessible parameters such as the concentration of Na stemming from the glass substrate or a precursor. For example, a relation between the Na content in the Mo layer and the formation of the $MoSe_2$ layer has been found.[4] Possibly, a diffusion of Mo into the absorber film, which was found for evaporated Mo on $CuInSe_2$ films with temperatures similar to those used during absorber fabrication,[8,18] might also play a role.

Until today the optimization of the back contact and even the choice of the used material have (with some exceptions, e.g., Ref. 19) generally been done empirically. This is mainly because a detailed investigation of the properties of the CIG(S)Se/Mo interface is difficult. A possible way to shed more light on this deeply buried interface is to lift the CIG(S)Se off the Mo layer, as demonstrated in the past.[10,11] In earlier publications we have demonstrated that this approach is suitable to make the buried CIG(S)Se/Mo interface accessible for investigation by surface-sensitive techniques and/or techniques that are sensitive to the surface-near bulk.[20,21] In this paper, we systematically investigate the impact of S incorporation in the CIG(S)Se on the CIG(S)Se/Mo-interface formation by x-ray photoelectron spectroscopy (XPS) and x-ray-excited Auger-electron spectroscopy (XAES) and paint a comprehensive picture of the chemical structure of the CIG(S)Se/Mo interface.

II. EXPERIMENT

This investigation is based on two classes of samples, namely, S-free CIGSe/Mo/glass and S-containing CIGSSe/Mo/glass structures. The chalcopyrite films (approximately 2 μm thick) were prepared using multisource (four for CIGSe and five for CIGSSe) thermal coevaporation. All CIG(S)Se films were deposited with uniform, Cu-deficient fluxes throughout the deposition process. The substrate was a soda-lime glass covered with a sputter-deposited Mo layer (approximately 0.7 μm), which was held at 550 °C during absorber formation (see Ref. 22 for more details). In order to minimize sample contamination due to air exposure, the samples were sealed under dry nitrogen immediately after preparation at IEC, limiting the exposure time to ambient air to less than 5 min. At UNLV, the samples were unpacked in a glovebag/glovebox under nitrogen atmosphere, directly in-

troduced into our ultrahigh-vacuum (UHV) system, and then the (air-exposed) sample surface ("absorber front") was characterized.

For the lift-off procedure, the samples (roughly 12 $\times$ 12 mm^2) were first removed from the vacuum system and glued with their CIG(S)Se front side to a stainless-steel plate using a conductive (Ag-containing) UHV-compatible epoxy glue. The glue was cured at slightly elevated (40–60 °C) temperature for several hours. Then, the samples were reintroduced into the N_2-filled glovebox, cleaved, and directly transferred back into the UHV system. During cleavage, the front part [stainless-steel plate/CIG(S)Se] of the structure was lifted off the back part [Mo/glass], exposing two freshly cleaved surfaces ["CIG(S)Se back" and "Mo side"]. A number of lift-off experiments for each sample class (CIGSe and CIGSSe) were done with subsequent XPS characterization, and only the results from those cleavage samples are considered here, where the lift-off process was successful leaving behind clean cleavage plane areas larger than the XPS probing area ($\sim$1 cm^2). In the following, the three "surfaces" for each sample class (S-free and S-containing) will be called: [I] "CIG(S)Se front," [II] "CIG(S)Se back," and [III] "Mo side."

For the XPS measurements, Mg $K\alpha$ and Al $K\alpha$ excitations and a Specs PHOIBOS 150MCD electron analyzer were used. The base pressure was in the 10^{-10} mbar range. The electron spectrometer was calibrated according to Ref. 23 using XPS and Auger line positions of different metals (Cu, Ag, and Au). For quantitative analysis, we fitted the different spectral photoemission contributions by Voigt functions and a linear background. The fit was performed simultaneously for all spectra of one sample class (i.e., S-free or S-containing chalcopyrite films). Several general constraints were applied (unless otherwise noted): for a given line, the full width at half maximum (FWHM) was coupled for all samples within one sample class. Furthermore, the FWHM for both peaks of a spin-orbit doublet was coupled, and the intensity ratio of the two peaks was set according to their multiplicity $(2j+1)$. For our quantitative considerations, only photoemission lines with similar kinetic energy (E_{kin}) were used, and thus we assume that the analyzer transmission and the information depth are also similar. In order to determine concentration ratios we therefore only corrected the area ratios of the photoemission lines by the corresponding photoionization cross sections.[24] In order to estimate the thickness of the $Mo(S_ZSe_{1-Z})_2$ layer formed at the CIGSSe/Mo interface (see below) from our XPS data, we used the inelastic mean-free path (λ=2.0 nm) of the Mo 3*d* photoelectrons in MoS_2, as calculated by the TPP-2 formula[25] using the QUASES code [relative uncertainty $\sim$20% (Ref. 26)] and $I = I_0 \cdot e^{-(d/\lambda)}$, where I is the intensity of the respective (attenuated) photoemission signal, I_0 is the unattenuated signal intensity of the Mo substrate, and d is the thickness of the attenuating $[Mo(S_ZSe_{1-Z})_2]$ layer.

III. RESULTS AND DISCUSSION

The XPS survey spectra of the CIGSe and CIGSSe samples are shown in Fig. 1. First, we find photoemission lines associated with Mo, Cu, In, Ga, S, and Se (as expected). Second, all surfaces also exhibit O and C signals. Due to the inert atmosphere during sample cleavage, surfaces [II] and [III] exhibit a smaller amount of adsorbed oxygen (O 1*s*, binding energy $E_B \sim 530$ eV) than the air-exposed CIG(S)Se front [I] [note that after a mild Ar^+-sputter treatment (50 eV, 1 $\mu A/cm^2$) the intensity of the O 1*s* as well as the C 1*s* XPS peaks decrease to only trace amounts]. This finding also explains the overall higher intensities of the absorber peaks for the CIG(S)Se back [II] compared to those of the CIG(S)Se front [I] due to smaller attenuation by surface adsorbates. The significant amount of carbon (C 1*s*, $E_B \sim 285$ eV) found on the cleaved surfaces points to carbon impurities incorporated at the interface. This is also confirmed by the C 1*s*:O 1*s* peak ratio, which is higher for the cleaved surfaces ([II] and [III]) than for the air-exposed CIG(S)Se front [I] for both sample classes. Third, it can be observed that the Na intensity (Na 1*s*, $E_B \sim 1072$ eV) at the CIGSe front is approximately six times higher than that at the CIGSSe front and that both front sides have a higher Na content than their respective back sides (approximately 1.8 $\times$ for CIGSe and 2.6$\times$ for CIGSSe, as derived from the corresponding detail spectra, not shown). In particular the latter point is surprising since, in our case, Na in the CIG(S)Se stems from the glass substrate [i.e., closer to the

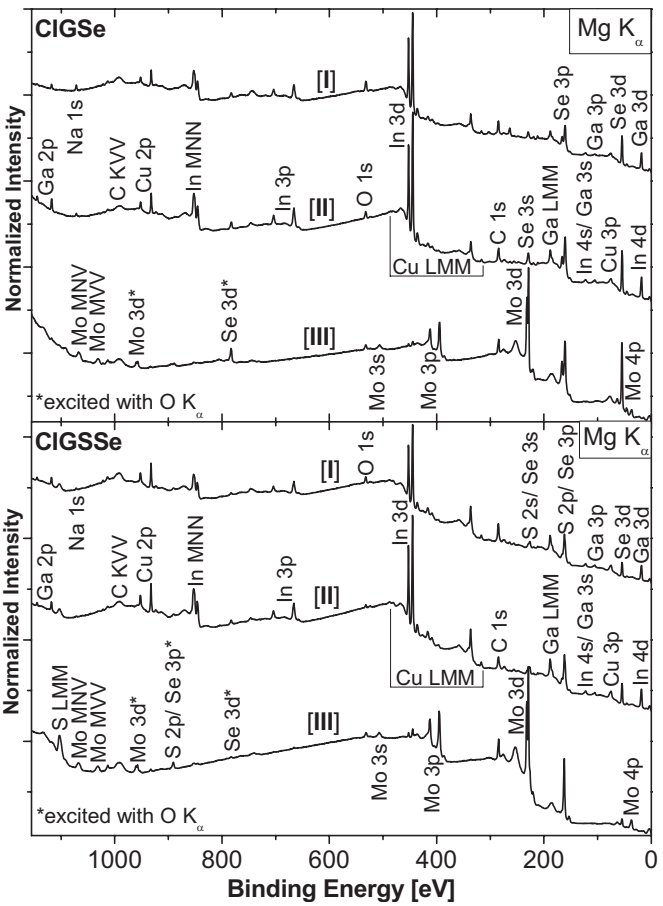

FIG. 1. XPS survey spectra of the investigated surfaces: CIG(S)Se front [I], CIG(S)Se back [II], and Mo side [III] for the CIGSe (top) and CIGSSe (bottom) sample set.

CIG(S)Se back side]. Fourth, the Mo 3*d* double peak ($E_B \sim 230$ eV) is only prominent in the Mo-side spectra [III] but not in those of the CIG(S)Se back [II] (note that the S 2*s*/Se 3*s* XPS lines are observed at a very similar energy), indicating that (in first approximation) the primary cleavage plane lies at the CIG(S)Se/Mo interface (as already shown in Ref. 20). This is corroborated by the fact that no strong CIG(S)Se-related XPS lines can be observed on the Mo-side spectra [III].

In order to derive the fraction of CIG(S)Se crystallites remaining on the Mo-side samples (in our previous experiments,[20] we derived that almost half of the Mo side was covered with absorber crystallites after lift-off), we analyzed the respective XPS detail spectra of the most prominent absorber elements (Ga $2p_{3/2}$, Cu $2p_{3/2}$, and In $3d_{3/2}$). The corresponding spectra of the Mo-side samples are shown in Fig. 2 (bottom spectra). It can be observed that all absorber elements are also present at the Mo side of the cleaved samples, albeit at much lower concentration than at the CIG(S)Se back (top spectra in Fig. 2). Comparing the intensity of the Cu $2p_{3/2}$ XPS line of the Mo side with that of the CIG(S)Se back, it can be approximated that at most only 2% (10%) of the Mo is covered with residual CIGSe (CIGSSe) crystallites, respectively, indicating a high quality of the cleavage process.

The comparison of the Cu, In, and Ga XPS line intensities of the Mo side (Fig. 2, bottom spectra) with those of the CIG(S)Se back (Fig. 2, top spectra) further shows that the relative abundance of Cu, In, and Ga on the Mo side significantly deviates from the stoichiometry of the CIG(S)Se back [note that all peaks in Fig. 2 are normalized to the respective peak of the CIG(S)Se back]. In both cases (more pronounced for CIGSe), an abundance of Ga is found on the Mo side. Compared to the corresponding Cu $2p_{3/2}$ intensity, for example, the Ga $2p_{3/2}$ intensity of the CIGSe (CIGSSe) sample is eight (two) times higher. This Ga accumulation (which we have previously inferred from x-ray emission spectroscopy data)[21] points either to a "diffusion" of Ga into the Mo film, a formation of a Ga-containing component [such as Ga_mSe_n or $Ga_m(S,Se)_n$] at the Mo surface, or the combination thereof.

Further, we have analyzed the Cu/(In+Ga) ratio, as determined from the respective intensity ratio of the Cu 3*p*, Ga 3*d*, and In 4*d* XPS signals (not shown) and corrected by the respective photoionization cross sections. We find that the surface stoichiometry of the CIG(S)Se front and of the CIG(S)Se back for both, the CIGSe and CIGSSe samples, is Cu poor compared to their nominal Cu:(In+Ga):(S+Se) =1:1:2 bulk composition. While the presence of a Cu-poor surface composition in high-efficiency CIG(S)Se solar cells[27] is widely accepted, only the pioneering work of Scheer and Lewerenz[11] and our own work report a Cu-poor stoichiometry at the $CuInS_2$ or CIGSe back side.[20] It is, however, not clear whether the absorber back side is inherently Cu-poor or whether the Cu-poor surface composition is only developed after cleavage.

In the following, we will focus on the XPS detail spectra of the Mo 3*d* photoemission line in order to also judge the quality of the cleaved CIG(S)Se back and to determine the chemical environment (as well as the amount) of Mo. The respective spectral region for the CIG(S)Se front [I], the CIG(S)Se back [II], and the Mo side [III] is shown in the left graph of Fig. 3 (Fig. 4) for the CIGSe (CIGSSe) sample set, respectively. Below each spectrum, the enlarged (three times) residual, i.e., the difference between the data and the fit, is shown. A comparison between the CIG(S)Se front and Mo-side spectra shows that the Mo 3*d* signal overlaps with the Se 3*s* (and S 2*s*) XPS lines. In the case of an ideal cleavage [and no composition gradients through the CIG(S)Se] one would expect the spectra for the CIG(S)Se front and the CIG(S)Se back to be very similar. As can be observed in Figs. 3 and 4 (left), this is not the case. In order to understand the differences, the respective spectra were simultaneously fitted for the CIGSe and CIGSSe samples, as described in the experimental section.

First, we discuss the fit results for the CIGSe samples (Fig. 3, left). In this fit, the FWHMs of the Mo $3d_{3/2}$ and $3d_{5/2}$ peaks were treated separately because of the well-known difference in core-hole lifetime (Coster-Kronig process).[28] To obtain a reasonable description of the Se 3*s*/Mo 3*d* peak structure for samples [II] and [III] (i.e., the two spectra in which both elements are present, but one of them is strongly dominant), we derived the Se/Mo ratio from the (nonoverlapping) Se 3*d* and Mo 4*p* lines (not shown). The Se 3*d*/Mo 4*p* peak ratio was corrected by the appropriate photoionization cross sections and the resulting

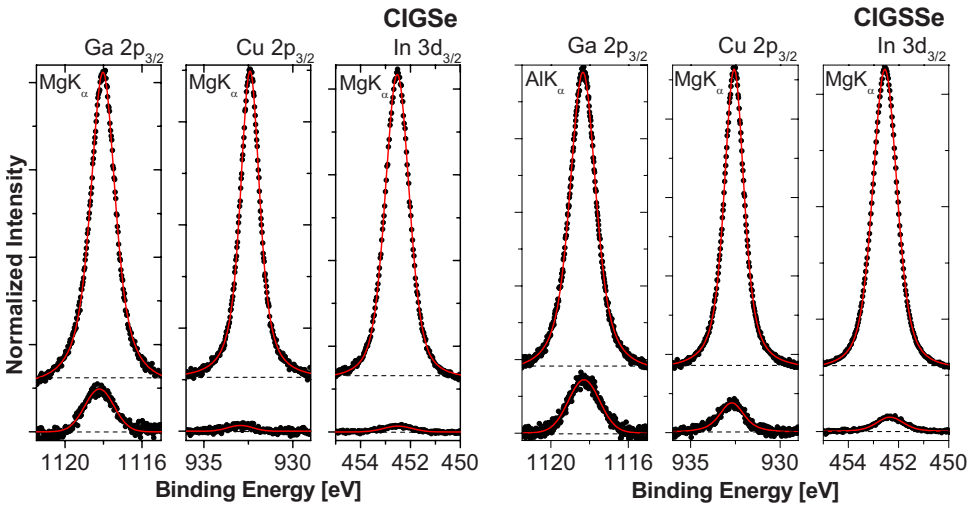

FIG. 2. (Color online) Detail spectra of the most prominent absorber XPS signals for the CIG(S)Se back (top spectra) and Mo-side (bottom spectra) samples of the CIGSe (left) and CIGSSe (right) test structures. The intensity of all XPS signals was normalized to the respective CIG(S)Se back spectrum for comparison. The experimental data and corresponding fits are shown as bullets and (red) solid lines, respectively.

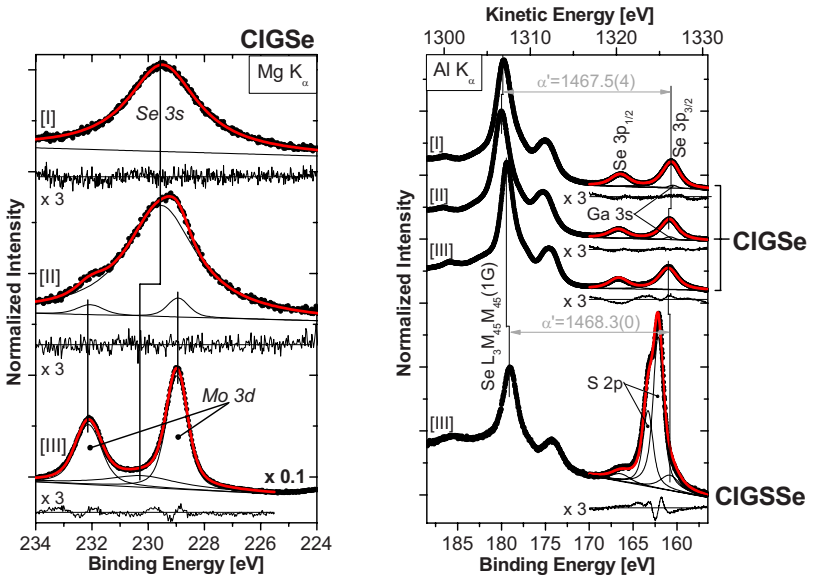

FIG. 3. (Color online) (Left): spectral region of the Se 3*s* and Mo 3*d* photoemission peaks for the CIGSe sample set (CIGSe front [I], CIGSe back [II], and Mo side [III]). The experimental data and corresponding fits are shown as bullets and (red) solid lines, respectively. Below each spectrum, the enlarged (three times) residual, i.e., the difference between the data and the fit, is shown. (Right): Se LMM Auger and Se 3*p* photoemission signal for the CIGSe sample set (CIGSe front [I], CIGSe back [II], and Mo side [III]; upper three spectra). For comparison, the corresponding CIGSSe Mo side spectrum (bottom) is also shown. Note that for the latter the Se 3*p* signal partially overlaps with the S 2*p* photoemission line. The experimental data and corresponding fits are shown as bullets and (red) solid lines, respectively. Below each spectrum, the enlarged (three times) residual, i.e., the difference between the data and the fit, is shown. The given numbers have an uncertainty of ± 0.05 eV and represent the modified Auger parameter α' (Se)$=E_{\mathrm{kin}}[\mathrm{Se}\,L_3M_{45}M_{45}(1G)]+E_B(\mathrm{Se}\,3p_{3/2})$.

Se/Mo ratio was used as a fixed parameter in the fit of the Se 3*s*/Mo 3*d* peak structure. The fits in Fig. 3 (left) reveal that the "CIGSe back" spectra can be very well described as a superposition of a Se 3*s* signal stemming from the CIGSe and a small Mo 3*d* contribution. Thus, either crystallites from the Mo-side remain on the CIGSe back (i.e., similar to the remaining CIGSe crystallites on the Mo-side surface) or Mo "diffuses" into the CIGSe layer (as suggested in Refs. 8, 18, and 29). Based on the present data, we are not able to distinguish between the two "Mo scenarios" but would consider the first scenario to be more likely. Note that a combination of these two (extreme) scenarios is also possible. In the first Mo scenario, we can compare the Mo 3*d* signal of the CIGSe back with that of the Mo side (note the scaling factor of $\times 0.1$ in spectrum [III]) and find that 1.6% of the CIGSe back would be covered by Mo-side crystallites (for this approximation, we took into account that the Mo-side sample is partially covered with absorber crystallites as discussed above). In the second Mo scenario, we can compute a Mo-doping concentration in the CIGSe back of 2.6×10^{20} cm^{-3} (see Ref. 30 for more details on this estimate), which is rather high but in the same order of magnitude as the reported numbers for Mo diffusion into $CuInSe_2$ films.[18]

As mentioned above, the Se/Mo ratio for the Mo side of the CIGSe sample $[2.0(7) \pm 0.1]$ was determined from the photoionization cross-section-corrected Se 3*d*/Mo 4*p* intensity ratio. The good quality of the Se 3*s*/Mo 3*d* fit in Fig. 3 (left) suggests that this value is indeed correct. Furthermore, it is in good agreement with earlier reports of the formation of a $MoSe_2$ layer at the CIGSe/Mo interface.[4,8–10,12,13,15,16] The comparison of the position of the Mo $3d_{5/2}$ $[E_B=(228.93 \pm 0.02)$ eV] and Se $3d_{5/2}$ $[E_B=(54.53 \pm 0.02)$ eV] XPS lines with literature values[31,32] for $MoSe_2$ $[E_B(\mathrm{Mo}\,3d_{5/2})=228.3-229.0$ eV, $E_B(\mathrm{Se}\,3d)=54.2-54.6$ eV] is also consistent with the formation of a $MoSe_2$ layer. In order to confirm that the selenium found on the Mo-side sample is in a different chemical environment than that of the CIGSe front and CIGSe back samples, we computed the corresponding modified Auger parameter α' (Fig. 3, right). Since α' is the sum of the kinetic energy of a specific Auger line and the binding energy of a specific photoemission signal {in our case α' (Se) $=E_{\mathrm{kin}}[\mathrm{Se}\,L_3M_{45}M_{45}(1G)]+E_B(\mathrm{Se}\,3p_{3/2})$}, it is not influenced by sample charging or variations in surface band bending. As can be observed in Fig. 3 (right), α' is the same $\{[1467.5(4) \pm 0.05]$ eV$\}$ for the CIGSe front and CIGSe back samples, indicating a similar chemical environment for Se. In contrast, it significantly differs for the Mo-side sample $\{[1468.3(0) \pm 0.05]$ eV$\}$. Note that no α' (Se) values for $MoSe_2$ or CIGSe can be found in the literature for comparison.

In order to shed light on the impact of the presence of sulfur on the chemical structure of the CIG(S)Se/Mo interface, we now discuss the fit results for the respective Se 3*s*/S 2*s*/Mo 3*d* region of the CIGSSe samples (Fig. 4, left). Because of the increased number of overlapping lines (compared to the CIGSe case), further constraints beyond the above-described fit procedure are needed. The Se/S ratio as derived from the photoionization cross-section-corrected Se $3p_{3/2}$/S $2p_{3/2}$ peak ratio (fit shown in Fig. 4, right) was used as a fixed parameter in the fit of the Se 3*s*/S 2*s*/Mo 3*d* peak structure. This constraint is especially important for

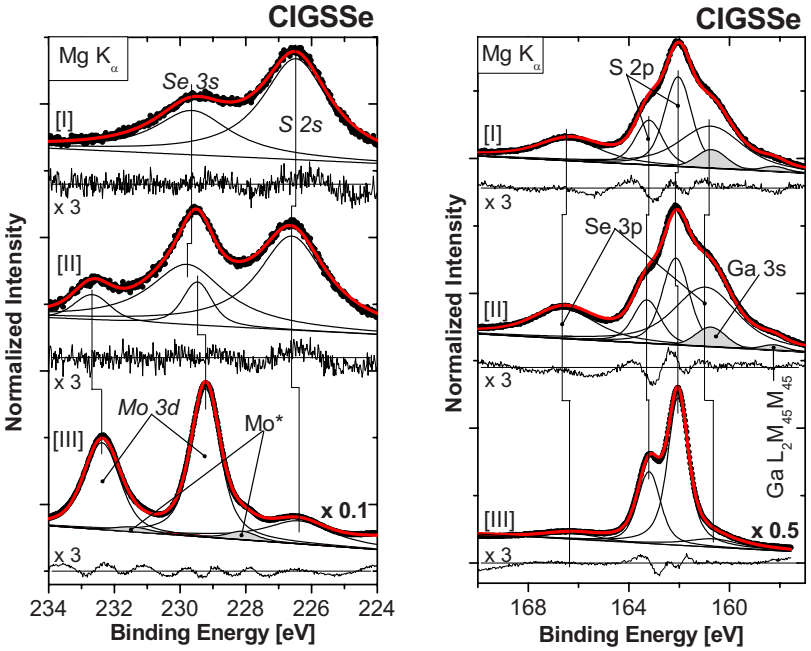

FIG. 4. (Color online) (Left): spectral region of the Se 3*s*, S 2*s*, and Mo 3*d* photoemission peaks for the CIGSSe sample set (CIGSSe front [I], CIGSSe back [II], and Mo side [III]). The experimental data and corresponding fits are shown as bullets and (red) solid lines, respectively. Below each spectrum, the enlarged (three times) residual, i.e., the difference between the data and the fit, is shown. The spectral contribution from a second molybdenum species is marked with Mo*. (Right): spectral window of the Se 3*p* and S 2*p* photoemission signals for the CIGSSe sample set (CIGSSe front [I], CIGSSe back [II], and Mo side [III]). The experimental data and corresponding fits are shown as bullets and (red) solid lines, respectively. Below each spectrum, the enlarged (three times) residual, i.e., the difference between the data and the fit, is shown.

the fit of the Mo-side spectrum because of the dominating Mo 3*d* photoemission signal. For the overlapping Se 3*p*/S 2*p* spectra, additional constraints were introduced. First, the spin-orbit splitting of the Se 3*p* (S 2*p*) photoemission peaks was set to 5.60 eV (1.15 eV) (Ref. 31) and, second, the Ga 3*s*/Se $3p_{3/2}$ intensity ratio was set according to the Ga/Se ratio determined from the photoionization cross-section-corrected Ga 3*d*/Se 3*d* peak ratio (fit not shown). The Se/S ratio was then derived to 0.5(2), 0.7(6), and 0.1(0) (all values ± 0.1) for the CIGSSe front, the CIGSSe back, and the Mo side, respectively. These Se/S ratios, together with the Se/Mo ratio of $0.1(8) \pm 0.1$ for the Mo side of the CIGSSe sample (derived from the photoionization cross-section-corrected Se 3*d*/Mo 4*p* intensity ratio, fit not shown), were then used as constraints for the fit of the Se 3*s*/S 2*s*/Mo 3*d* peak structure in Fig. 4 (left). This fit now allows us to directly identify the differences of the chemical structure at the CIGSSe/Mo interface compared to the CIGSe/Mo interface. We find a S/Mo ratio of $1.8(2) \pm 0.1$ for the CIGSSe Mo side (as determined from the photoionization cross-section-corrected S 2*s*/Mo $3d_{5/2}$ intensity ratio). This points to the formation of a $Mo(S_ZSe_{1-Z})_2$ layer with $Z=0.9(1)$ at the CIGSSe/Mo interface. Comparing the position of the Mo $3d_{5/2}$ [$E_B=(229.23 \pm 0.02)$ eV] and S $2p_{3/2}$ [$E_B=(162.05 \pm 0.02)$ eV] XPS lines with literature values[30,31] for MoS_2 [E_B(Mo $3d_{5/2}$)=228.8–230.2 eV, E_B(S $2p_{3/2}$)=161.5–162.9 eV] further confirms the formation of a S-rich (i.e., MoS_2-dominated) $Mo(S_ZSe_{1-Z})_2$ layer. The energetic position of the Se $3d_{5/2}$ photoemission line of the CIGSSe Mo-side sample [$E_B=(54.40 \pm 0.02)$ eV] agrees well with that of $MoSe_2$ (see above) and the modified Auger parameter {[1468.3(0) $\pm$ 0.05] eV see Fig. 3 (right)} is the same as that for the $MoSe_2$ layer formed at the CIGSe/Mo interface. Both indicates that the Se atoms in the S-rich $Mo(S_ZSe_{1-Z})_2$ layer are still in a similar chemical environment as the Se atoms in pure $MoSe_2$. The fit in Fig. 4 (left) also shows that the CIGSSe back spectrum can be very well described as a superposition of Se 3*s* and S 2*s* XPS signals stemming from the CIGSSe and a Mo 3*d* contribution from the Mo side (similar to the CIGSe back spectrum). Based on the hypothesis that crystallites from the Mo side remain on the CIGSSe back during lift-off, the comparison of the CIGSSe back Mo 3*d* signal with that of the Mo side (note the scale factor of $\times 0.1$ for the Mo-side spectrum) reveals that 2.6% of the CIGSSe back is covered by Mo-side crystallites. In the case of a potential Mo diffusion into the CIGSSe layer (see above), this would correspond to an estimated Mo-doping concentration in the CIGSSe back of 5.0×10^{20} cm^{-3},[30] which again agrees well with doping concentrations reported elsewhere.[18]

As mentioned above, the Se/S ratio of the $Mo(S_ZSe_{1-Z})_2$ does not mirror that of the CIGSSe back sample [0.1(0) vs 0.7(6)]. The formation of MoS_2 during the preparation of the CIGSSe film is apparently preferred over the formation of $MoSe_2$, which agrees well with the corresponding (room-temperature) Gibbs energies of formation [$\Delta G_f^0(MoS_2)$ =−266.5 kJ/mol and $\Delta G_f^0(MoSe_2)$=−225.2 kJ/mol (see Ref. 33 for more details)].

Careful inspection of the CIGSSe Mo-side spectrum and its corresponding fit reveals that an additional Mo species

(Mo* in Fig. 4, left) can be observed. Since the energetic position of the respective Mo $3d_{5/2}$ line [$E_B = (228.11 \pm 0.02)$ eV] is in good agreement with the literatures values[31,32] for metallic Mo [E_B(Mo $3d_{5/2}$) $= 227.4-228.6$ eV], we conclude that the $Mo(S_ZSe_{1-Z})_2$ layer either does not cover the (initial) Mo layer completely or, more likely, that it is thinner than the $MoSe_2$ layer observed at the CIGSe/Mo interface, where no XPS Mo $3d$ feature ascribed to metallic Mo can be found. In the latter case and under the assumption that the Mo $3d_{5/2}$ photoelectrons are exclusively attenuated in a pure, homogeneous MoS_2 layer, we can estimate the thickness of the $Mo(S_ZSe_{1-Z})_2$ layer to be approximately 8 ± 2 nm (see Ref. 34 for more details). The thickness difference between the $Mo(S_ZSe_{1-Z})_2$ and the $MoSe_2$ films might be related to the observed lower Na concentration at the CIGSSe front and CIGSSe back compared to that of the corresponding CIGSe samples (see discussion above)—a similar finding was first pointed out by Kohara *et al.*,[4] who observed that a $MoSe_2$ layer is formed at the CIGSe/Mo interface only if Na is present during the interface formation.

The findings discussed in conjunction with Figs. 1–4 are summarized schematically in Fig. 5. The primary cleavage plane is (as already elaborated in Ref. 20) located at the CIG(S)Se/Mo interface (identified by the solid red line in Fig. 5) and an interfacial $MoSe_2$ [$Mo(S_ZSe_{1-Z})_2$] layer is formed between CIGSe (CIGSSe) and Mo. The $Mo(S_ZSe_{1-Z})_2$ is thinner than the $MoSe_2$ layer, as depicted in the detailed schemes in Fig. 5. The observed Mo signal at the CIG(S)Se back surface and the Ga accumulation at the Mo-side surface can be explained by two extreme scenarios (or combinations thereof). The "diffusion scenario" [(a) schemes in Fig. 5] assumes a Mo and Ga diffusion into the CIG(S)Se back and Mo-side surfaces, respectively. The "residue scenario" [(b) schemes in Fig. 5] explains the observation of Mo and Ga on the "opposite" surfaces by residual Mo-side crystallites remaining on the CIG(S)Se back after cleavage and the formation of a Ga compound [Ga_mSe_n or $Ga_m(S,Se)_n$] at the CIG(S)Se/Mo interface. These two different scenarios are shown for the CIGSe/Mo and CIGSSe/Mo interfaces in schemes "1" (left) and "2" (right), respectively.

As mentioned, we find an eightfold (twofold) enhancement of Ga at the CIGSe (CIGSSe) Mo side compared to the corresponding CIG(S)Se back. In the diffusion scenario the resulting different doping concentration is presented as a different effective layer thickness. For that a homogenous doping profile of identical concentration for the CIGSe and CIGSSe systems was assumed. In order to account for the different Ga amount, the (a) schemes in Fig. 5 hence show a thicker Ga-doped layer for CIGSe than for CIGSSe. As already discussed, we find a similar trend for the thickness of the interfacial $MoSe_2$ and [$Mo(S_ZSe_{1-Z})_2$] layer, and thus we speculate [as shown in the (a) schemes of Fig. 5] that the Ga only diffuses into the Mo chalcogenide interlayer. For the residue scenario [(b) schemes in Fig. 5] the observed higher Ga concentration at the CIGSe back compared to that at the CIGSSe back is represented by a Ga_mSe_n layer that is thicker than the $Ga_m(S,Se)_n$ layer.

For the diffusion scenario we have to additionally consider that not only a Ga accumulation is found on the Mo side but that also a Mo signal is detected at the CIG(S)Se back surfaces. Again representing the dopant concentration as an effective thickness (as discussed above for the "Ga doping"), the CIGSe:Mo layer is shown thinner than the CIGSSe:Mo layer [(a) schemes of Fig. 5], corresponding to the Mo doping in the CIGSe back (CIGSSe back) samples of 2.6×10^{20} cm^{-3} (5.0×10^{20} cm^{-3}). Although the schemes are not drawn to scale, the relative thickness of the different layers is thus related to the amount of Mo (Ga) found at the CIG(S)Se back (Mo-side) surface and to the thickness of the interfacial $MoSe_2$ [$Mo(S_ZSe_{1-Z})_2$] layer found at the Mo/CIGSe (Mo/CIGSSe) interface, respectively. Note that the described scenarios are two extreme explanations for our findings. In fact, the real chemical structure of the CIG(S)Se/Mo interface might also be a superposition of the situations described by the diffusion and residue scenarios.

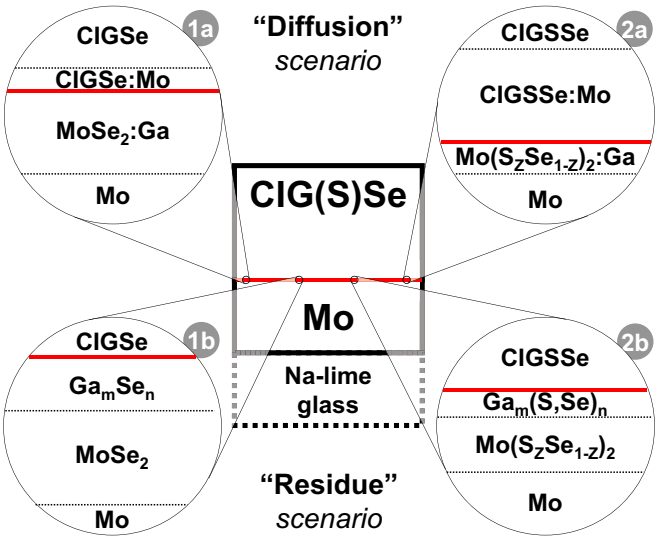

FIG. 5. (Color online) Schemes visualizing the different chemical structure scenarios at the CIGSe/Mo [schemes in (1a) and (1b)] and CIGSSe/Mo [schemes in (2a) and (2b)] interfaces. While the (a) schemes represent the diffusion scenarios, for the (b) schemes it was assumed that the reason for the Mo found on the "absorber back" samples is trivial (remaining back-contact crystallites) and that the found Ga accumulation on the Mo-side samples is indicative for the formation of a Ga compound [Ga_mSe_n or $Ga_m(S,Se)_n$]. Although the schemes are drawn not to scale, the relative thickness of the different layers is related to the amount of Mo (Ga) found on the CIG(S)Se back (Mo-side) samples and to the thickness of the interfacial $MoSe_2$ [$Mo(S_ZSe_{1-Z})_2$] layer found at the Mo/CIGSe ([Mo/CIGSSe] interface, respectively.

IV. SUMMARY

We have systematically investigated the chemical properties of the Cu(In,Ga)Se_2/Mo and Cu(In,Ga)$(S,Se)_2$/Mo interfaces. We have demonstrated how a suitable lift-off technique [which we find to primarily cleave the CIG(S)Se/Mo/glass structures at the CIG(S)Se/Mo interface] can be combined with powerful surface-sensitive spectroscopy (x-ray photoelectron and Auger-electron spectroscopy) to gain insight into the chemical structure of a rather complicated

metal/semiconductor interface. For the S-free CIGSe/Mo structure we find the formation of an interfacial $MoSe_2$ layer. The presence of S at that interface strongly influences the chemical composition of the Mo chalcogenide interlayer, resulting in the formation of a $Mo(S_ZSe_{1-Z})_2$ layer between CIGSSe and Mo. Based on our results, we conclude that the formation of MoS_2 during the preparation of the CIGSSe film is preferred over that of $MoSe_2$. At the CIG(S)Se back and Mo-side cleavage planes we find a Mo signal and an abundance of Ga, respectively, which can be explained by two extreme scenarios (or combinations thereof). While the diffusion scenario assumes a Mo and Ga diffusion, respectively, the residue scenario is based on residual Mo-side crystallites and the consequential though speculative formation of a Ga compound [Ga_mSe_n or $Ga_m(S,Se)_n$].

These observations point to pronounced chemical interactions and diffusion/intermixing processes taking place during CIG(S)Se formation on Mo substrates. This indicates that the processes at the CIG(S)Se/Mo interface are very complex, but a more detailed picture of the chemical structure is now available. The related consequences for the commonly used electronic back-contact model of chalcopyrite thin-film solar cell devices have to be reconsidered and must be addressed in future experiments.

ACKNOWLEDGMENTS

We acknowledge funding by the National Renewable Energy Laboratory under Subcontracts No. XXL-5-44205-12 and No. ADJ-1-30630-12. M.B. is additionally grateful for sponsorship by the Deutsche Forschungsgemeinschaft (DFG) within the Emmy-Noether-Programm.

*Corresponding author. FAX: +1-702-895-4072; baerm2@unlv.nevada.edu

[1] M. A. Green, K. Emery, Y. Hishikawa, and W. Warta, Prog. Photovoltaics **16**, 61 (2008).
[2] L. L. Kazmerski and G. A. Sanborn, J. Appl. Phys. **48**, 3178 (1977).
[3] A. J. Nelson, D. Niles, L. L. Kazmerski, D. Rioux, R. Patel, and H. Höchst, J. Appl. Phys. **72**, 976 (1992).
[4] N. Kohara, S. Nishiwaki, Y. Hashimoto, T. Negami, and T. Wada, Sol. Energy Mater. Sol. Cells **67**, 209 (2001).
[5] W. N. Shafarman and J. E. Phillips, Conference Record 25th IEEE Photovoltaic Specialists Conference (Cat. No. 96CH35897), Washington, DC, 1996, p. 917.
[6] P. E. Russell, O. Jamjoum, R. K. Ahrenkiel, L. L. Kazmerski, R. A. Mickelsen, and W. S. Chen, Appl. Phys. Lett. **40**, 995 (1982).
[7] T. Löher, C. Pettenkofer, and W. Jaegermann, First World Conference on Photovoltaic Energy Conversion/Conference Record 24th IEEE Photovoltaic Specialists Conference (Cat. No. 94CH3365-4), Hawaii, 1994, p. 295.
[8] S. Raud and M. A. Nicolet, Thin Solid Films **201**, 361 (1991).
[9] H. Sato, T. Hama, E. Niemi, Y. Ichikawa, and H. Sakai, *Proceedings to the Ninth International Conference of Ternary and Multinary Compounds* [Jpn. J. Appl. Phys., Suppl. **32**, 50 (1993)].
[10] D. Schmid, J. Kessler, and H. W. Schock, Proceedings of the 12th European Photovoltaic Solar Energy Conference, Amsterdam, Netherlands, 1994 (unpublished), p. 653.
[11] R. Scheer and H.-J. Lewerenz, J. Vac. Sci. Technol. A **13**, 1924 (1995).
[12] T. Wada, N. Kohara, T. Negami, and M. Nishitani, Jpn. J. Appl. Phys., Part 2 **35**, L1253 (1996); S. Nishiwaki, N. Kohara, T. Negami, and T. Wada, *ibid.* **37**, L71 (1998); T. Wada, N. Kohara, S. Nishiwaki, and T. Negami, Thin Solid Films **387**, 118 (2001).
[13] R. Takei, H. Tanino, S. Chichibu, and H. Nakanishi, J. Appl. Phys. **79**, 2793 (1996).
[14] J. Álvarez-García, A. Pérez-Rodríguez, A. Romano-Rodríguez, J. R. Morante, L. Calvo-Barrio, R. Scheer, and R. Klenk, J. Vac. Sci. Technol. A **19**, 232 (2001); V. Izquíerdo-Roca, A. Perez-Rodríguez, A. Romano-Rodríguez, J. R. Morante, J. Álvarez-García, and L. Calvo-Barrio, J. Appl. Phys. **101**, 103517 (2007).
[15] V. Probst, W. Stetter, W. Riedl, H. Vogt, M. Wendl, H. Calwer, S. Zweigart, K.-D. Ufert, B. Freienstein, H. Cerva, and F. H. Karg, Thin Solid Films **387**, 262 (2001).
[16] Th. Glatzel, D. Fuértes-Marron, Th. Schedel-Niedrig, S. Sadewasser, and M. Ch. Lux-Steiner, Appl. Phys. Lett. **81**, 2017 (2002); R. Würz, D. Fuertes Marrón, A. Meeder, A. Rumberg, S. M. Babu, Th. Schedel-Niedrig, U. Bloeck, P. Schubert-Bischoff, and M. Ch. Lux-Steiner, Thin Solid Films **431-432**, 398 (2003); D. Fuertes Marrón, A. Meeder, S. Sadewasser, R. Würz, and C. A. Kaufmann, Th. Glatzel, Th. Schedel-Niedrig, and M. Ch. Lux-Steiner, J. Appl. Phys. **97**, 094915 (2005).
[17] J. H. Scofield, A. Duda, D. Albin, B. L. Ballard, and P. K. Predecki, Thin Solid Films **260**, 26 (1995).
[18] T. D. Dzhafarov, M. S. Sadigov, E. Cingi, E. Bacaksiz, and M. Caliskan, J. Mater. Sci. Lett. **19**, 1521 (2000).
[19] K. Orgassa, H.-W. Schock, and J. H. Werner, Thin Solid Films **431-432**, 387 (2003).
[20] L. Weinhardt, O. Fuchs, A. Peter, E. Umbach, C. Heske, J. Reichardt, M. Bär, I. Lauermann, I. Kötschau, A. Grimm, S. Sokoll, M. Ch. Lux-Steiner, T. P. Niesen, S. Visbeck, and F. Karg, J. Chem. Phys. **124**, 074705 (2006).
[21] L. Weinhardt, M. Blum, M. Bär, C. Heske, O. Fuchs, E. Umbach, J. D. Denlinger, K. Ramanathan, and R. Noufi, Thin Solid Films **515**, 6119 (2007).
[22] M. Gossla and W. N. Shafarman, Thin Solid Films **480-481**, 33 (2005).
[23] D. Briggs and M. P. Seah, *Practical Surface Analysis* (Wiley, New York, 1990), Vol. 1.
[24] J. H. Scofield, J. Electron Spectrosc. Relat. Phenom. **8**, 129 (1976).
[25] S. Tanuma, C. J. Powell, and D. R. Penn, Surf. Interface Anal. **21**, 165 (1993).
[26] S. Tougaard, QUASES-IMP-TPP2M code for the calculation of the inelastic electron mean-free path, Version 2.2 (http://www.quases.com/).
[27] D. Schmid, M. Ruckh, F. Grunwald, and H.-W. Schock, J. Appl.

Phys. **73**, 2902 (1993).
[28] N. Mårtensson and R. Nyholm, Phys. Rev. B **24**, 7121 (1981).
[29] T. Dzhafarov, M. Sadigov, E. Cingi, E. Bacaksiz, and M. Caliskan, Jpn. J. Appl. Phys., Suppl. **39**, 194 (2000).
[30] According to the densities (ρ) and molar masses (M) for Mo, $MoSe_2$, and MoS_2 taken from the 87th Edition of the CRC Handbook of Chemistry and Physics 2006–2007 (http://www.hbcpnetbase.com/), the respective molar densities ($n=\rho/M$) can be calculated to 0.106, 0.027, and 0.032 mol/cm^3, respectively. Multiplication of the molar density of $MoSe_2$ [MoS_2] with the intensity ratio of the Mo 3*d* XPS signal of the "CIGSe [CIGSSe] back" and the Mo side (0.016 [0.026], see text) leads to the "Mo-doping" concentration (under the assumption that the doping profile is homogeneous within the information depth of XPS).
[31] NIST X-Ray Photoelectron Spectroscopy Database, NIST Standard Reference Database 20, Version 3.4 (http://srdata.nist.gov/xps/).
[32] C. D. Wagner, W. M. Riggs, L. E. Davis, and J. F. Moulder, in *Handbook of X-Ray Photoelectron Spectroscopy*, edited by G. E. Muilenberg (Perkin-Elmer, Eden Prairie, 1979).
[33] The Gibbs energy of formation for $MoSe_2$ (MoS_2) was determined for $T=298.16$ K according to $\Delta G_f^0=\Delta H_f^0-T\cdot\Delta S$. The enthalpy ΔH_f^0 for $MoSe_2$ (MoS_2) used for the calculations was −243.2 kJ/mol [−275.3 kJ/mol] taken from V. Ya. Leonidov and P. A. G. O'Hare, *Fluorine Calorimetry* (Begell House, New York, 1999), p. 194 [P. A. G. O'Hare, E. Benn, F. Yu Cheng, and G. Kuzmycz, J. Chem. Thermodyn. **2**, 797 (1970)]. The change in entropy $\Delta S_{MoSe_2/MoS_2}=S^0_{MoSe_2/MoS_2}-S^0_{Mo}-2\cdot S^0_{Se/S}$ was calculated from the standard entropies for the respective elements taken from http://www.qivx.com/ispt/ptw_st.php and $S^0_{MoSe_2}=83.3$ J/K mol [$S^0_{MoS_2}=62.6$ J/K mol] taken from A. V. Blinder, A. S. Bolgar, and Zh. A. Trofimova, Poroshk. Metall. (Kiev) **363**, 52 (1993) [D. R. Fredrickson and M. G. Chasanov, J. Chem. Thermodyn. **3**, 693 (1971)], resulting in $\Delta S_{MoSe_2}=-30.2$ J/K mol [$\Delta S_{MoS_2}=-29.7$ J/K mol].
[34] For the Mo 3*d* signal intensity reference of the bare (metallic) Mo layer (I_0, see Sec. II), we used the Mo 3*d* intensity of the S-rich $Mo(S_ZSe_{1-Z})_2$ contribution to the Mo-side spectrum [corrected by the molar ratio $n_{Mo}/n_{MoS_2}=3.3$ (see Ref. 30 for details)].